Received: 22 July 2021 | Revised: 20 September 2021 | Accepted: 20 October 2021

DOI: 10.1002/ame2.12186

ORIGINAL ARTICLE

Establishment of an oligoasthenospermia mouse model based on *TAp73* gene suppression

Hong-Juan Liu[1] | Meng-Yun Deng[1] | Yan-Yan Zhu[1] | De-Ling Wu[2] | Xiao-Hui Tong[1] | Li Li[1] | Lei Wang[1] | Fei Xu[1] | Tong-Sheng Wang[1,2]

[1]School of Integrated Traditional Chinese and Western Medicine, Anhui University of Chinese Medicine, Hefei, China

[2]Anhui Province Key Laboratory of Chinese Medical Formula, School of Pharmacy, Anhui University of Chinese Medicine, Hefei, China

Correspondence
Prof. Tong-Sheng Wang, School of Integrated Traditional Chinese and Western Medicine, Anhui University of Chinese Medicine, Hefei, China.
Email: wtsyl@163.com

Funding information
This project was supported by the Natural Science Foundation of Anhui Provincial Department of Education (no. KJ2020A0386) and National Natural Science Foundation of China (no. 82174162).

Abstract

Background: Oligoasthenospermia is one of the main causes of male infertility. Researchers usually use chemical drugs to directly damage germ cells to prepare oligoasthenospermia models, which disregards the adhesion and migration between spermatogenic cells and Sertoli cells. *TAp73* is a critical regulator of the adhesin of germ cell; thus, we sought to explore a novel oligoasthenospermia model based on *TAp73* gene suppression.

Methods: Mice in the Pifithrin-α group were injected intraperitoneally with 2.5 mg/kg Pifithrin-α (*TAp73* inhibitor) daily for 30 consecutive days. Reproductive hormone levels and epididymal sperm quality, as well as the network morphology of Sertoli cells were tested.

Results: Sperm density, motility, and the relative protein and mRNA expression of *TAp73* and *Nectin 2* were obviously decreased in the Pifithrin-α group compared with the normal control group. No significant distinction was observed in the relative mRNA and protein expression of *ZO-1*. Furthermore, the tight junctions (TJs) and apical ectoplasmic specialization (ES) were destroyed in the Pifithrin-α group.

Conclusion: The above results indicate that we successfully established a new oligoasthenospermia mouse model. This study provides a foundation for further exploration of the roles of *TAp73* genes during spermatogenesis and provides new research objects for further oligospermia research and future drug discovery.

KEYWORDS

ectoplasmic specialization, *Nectin 2*, oligoasthenospermia, *TAp73*, *ZO-1*

1 | INTRODUCTION

A survey by the World Health Organization shows that infertility is estimated to affect 10%–15% of couples, and approximately 50% of these couples are infertile because of male infertility.[1] Infertility might become the third disease affecting human health and life quality, behind tumors and cardiovascular disease.[2] With a gradual increase in incidence, male infertility has received increasing attention worldwide.[3] Oligoasthenospermia has become a major etiology of

Hong-Juan Liu, Meng-Yun Deng and Yan-Yan Zhu contributed equally to this manuscript.

male infertility.[4] However, the underlying molecular mechanism is unclear owing to the diversity in occurrence and complicated pathogenesis of oligoasthenospermia. This ultimately results in current treatments of oligoasthenospermia being mostly empirical and experimental, with a lack of effective treatment drugs and methods.[5] Therefore, there is an urgent need to study the mechanism of oligoasthenospermia and find a safe and effective treatment.

The establishment of an animal model that conforms to the clinical course and characteristics of diseases is a necessary condition for research on the mechanism of disease and for efficient therapeutic drugs. At present, researchers have developed an animal model of oligoasthenospermia using the reproductive toxicity of drugs such as *Tripterygium wilfordii* polyglycosides,[6] busulfan,[7] and cyclophosphamide. These drugs can directly disrupt spermatogonial stem cells or spermatids integrity.[8] Such models disregard the adhesion and migration between spermatogenic and Sertoli cells, and fail to truly simulate the entire process of spermatogenesis. Most of the current oligoasthenospermia models fail to identify the key role of Sertoli cells in spermatogenesis.

As crucial regulators of relevant adhesive factors in germ cells, *TAp73* genes play critical roles in modulating the adhesion and migration between spermatogenic and Sertoli cells. Knockout of *TAp73* causes severe depletion of mature spermatozoa, which suggests that knockdown of *TAp73* impairs adhesion and migration, thereby causing the untimely detachment of germ cells from the seminiferous epithelium.[9] Therefore, we used the repression of *TAp73* gene expression by Pifithrin-α, an inhibitor of *TAp73*,[10] to impede the adhesion and migration between spermatogenic and Sertoli cells, and establish a new mouse model of oligoasthenospermia. This model involves the intercellular interactions between Sertoli cells and spermatogenic cells, which is more consistent with pathological processes. Establishment of the model provides a new research object for identifying the molecular mechanism of specific biological processes and disease occurrence, as well as finding efficient therapeutic agents.

2 | MATERIALS AND METHODS

2.1 | Animals

C57BL/6 male mice were sourced from Zhejiang Ziyuan Laboratory Animal Technology Co. Ltd. The Animal Ethics Committee of Anhui University of Chinese Medicine approved all methods used in this study (approval no: AHUCM-mouse-2020039).

2.2 | Methods

Twenty-five-week-old C57BL/6 male mice were randomly assigned into 2 groups: normal control group and Pifithrin-α group ($n = 10$ per group). The Pifithrin-α group was treated with Pifithrin-α (2.5 mg/kg) by intraperitoneal injection, while the normal control group was given an equal volume of solvent for 30 consecutive days.

2.3 | Body weight growth curve and organ coefficient

Body weight was recorded every 3 days. After 30 days injection, mice were euthanized by cervical dislocation and tissues were rapidly extracted. Organ coefficient (%) = (organ weight/body weight) × 100%.

2.4 | Serum hormone levels

The eyeball was removed, and the blood sample was collected in a centrifuge tube. The serum was separated, and the hormone levels were measured by enzyme-linked immunosorbent assay (ELISA).[7] The following hormones were tested: follicle-stimulating hormone (FSH), luteinizing hormone (LH), and testosterone (T).

2.5 | Sperm quality

The epididymis was dissected into small pieces and incubated in 2 ml saline for 20 min at 37°C to release sperm, which was collected for counting, smear, and motility analysis. The sperm density was calculated using a Makler counting chamber (Israel). Sperm density = total number of sperm in 10 squares on the counting chamber × 10^6/ml. The motility of sperm was divided into 4 types: fast forward movement (A type), slow forward movement (B type), sway left and right in place (C type), and immobilized sperm (D type). Sperm motility = total A and B sperm/number of total sperm.[11]

2.6 | Sperm malformation rate

To assay sperm malformation rate, smears were prepared from the sperm suspension (10 μl) and stained with eosin stain. The morphology and quantity of abnormal sperm were observed and recorded under a high-power microscope, using a random observation of 500 sperm per sample. Abnormal sperm exhibited head or tail defects, such as non-hooked heads, double heads, tail rotation, or double tail deformity. The sperm malformation rate = number of malformed sperm/number of examined sperm.[11]

2.7 | Pathological changes in testicular and epididymal tissue (H&E)

Testicular and epididymal tissues were paraffin-embedded, dewaxed, rehydrated, and stained with hematoxylin and eosin (H&E).

Images were captured by optical microscope and examined for pathological changes.[12]

2.8 | Testicular ultrastructure

Fresh testicular tissues were immersed in 2.5% glutaraldehyde solution overnight at 4°C. Following fixation, testicular tissues were washed with phosphate-buffered saline (PBS). Then testicular tissues were immersed in 1% osmium tetroxide solution for 2 h at room temperature. After that, they were stained overnight with saturated uranyl acetate in 70% ethanol at 4°C. Testicular tissue was transited with propylene oxide and embedded in the epoxy resin, Epon812. The samples were then cut into ultrathin sections, which were trimmed and cut into serial sections of 50–70 nm positioned by methylene blue staining under an optical microscope. Finally, the ultrathin slides were stained with lead citrate and observed under a transmission electron microscope.[13]

2.9 | Sperm apoptosis rate

The epididymis was dissected into small pieces and incubated in 2 ml saline for 20 min at 37°C. Subsequently, it was centrifuged and the supernatant was discarded. The precipitated spermatozoa were washed twice with PBS. Annexin V binding solution (400 μl) was added to resuspend the spermatozoa. Apoptotic sperm cells were determined by Annexin-V-fluorescein isothiocyanate (FITC)/PI double staining (BestBio, China), and the apoptosis rate was determined using flow cytometry. The total apoptosis rate was calculated as the sum of the early and late apoptosis rates.[14]

2.10 | Spermatogenic cell apoptosis

Following 24 h of fixation in 4% paraformaldehyde fixative, testes tissues were dehydrated and embedded. Then samples were cut into 5-μm sections. A TUNEL kit (Abbkine, China) was employed to examine apoptotic cells. The TUNEL–positive apoptotic cells were observed as brown cells, while normal cells had a blue nucleus. A minimum of 500 cells per slice were counted.[15]

$$\text{Apoptosis rate}(\%) = (\text{number of apoptotic cells})/500 \times 100\%.$$

2.11 | The relative mRNA expression levels of *TAp73* and adherence factors in testis

Trizol reagent was used for RNA isolation using testis tissues. The isolated RNA was subsequently reverse transcribed into cDNA (Thermo Fisher Scientific, China). This was followed by quantitative real-time PCR using a SYBR Green dye (Biosharp, China). Primers were used as described in Table 1. The PCR program consisted of 40 cycles of 95°C for 15 s, 55°C for 15 s, and 72°C for 30 s. Relative gene expression was performed using the comparative $2^{-\Delta\Delta Ct}$ method.[16]

TABLE 1 Primer sequences

Gene name	Primer sequence
TAp73	
Forward	CATCCCTTCCAATACCGACTAC
Reverse	CTTCAAGAGTGGGGAGTATGTC
ZO-1	
Forward	CTGGTGAAGTCTCGGAAAAATG
Reverse	CATCTCTTGCTGCCAAACTATC
GAPDH	
Forward	AGGCCGGTGCTGAGTATGTC
Reverse	TGCCTGCTTCACCACCTTCT
Nectin 2	
Forward	GCATCATTGGAGGTATTATCGCT
Reverse	GAGGGAGGTCCTTCCAGTTC

2.12 | The relative protein expression levels of TAp73 and adherence factors

Total protein of testicular tissues was extracted using RIPA lysis buffer. The protein content of samples was measured using a BCA protein assay kit (Beyotime, China). Quantified protein supernatant was mixed with 5× protein loading buffer proportionally, then the sample was boiled at 100°C for 6 min. The expression of TAp73, Zo-1, and Nectin-2 proteins was determined via western blot analysis. Quantification of protein bands was done with Image J software.[16]

2.13 | Data analysis and statistics

All data were represented as the mean ± standard deviation and analyzed using SPSS software 17.0, with $p \leq .05$ indicating significance.

3 | RESULTS

3.1 | Body weight growth curve and organ coefficient

There was no significant difference in mice body weight between the control group and the Pifithrin-α group (Figure 1A). The coefficients of epididymis decreased significantly in the Pifithrin-α group compared with that the normal control group ($p < .05$), whereas no significant differences were observed in other organ coefficients (Figure 1B).

3.2 | Serum hormone levels of T, FSH, and LH

Compared with the normal control group, levels of T and FSH were significantly decreased, while the level of LH was significantly increased in the Pifithrin-α group ($p < .05$) (Figure 2).

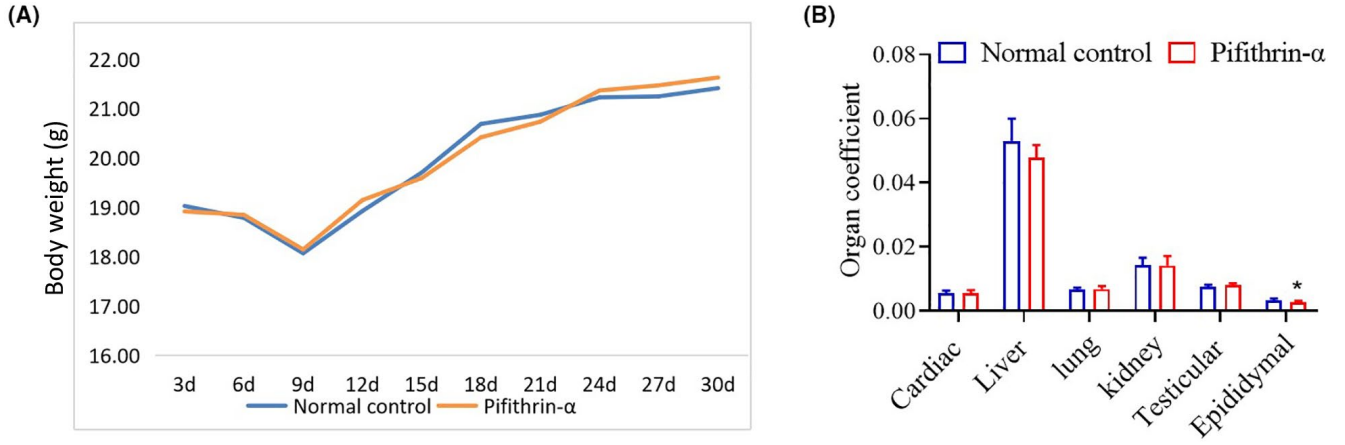

FIGURE 1 Effects of Pifithrin-α on the mouse body weight and organ coefficient. (A) No significant difference in mouse body weight between the normal control group and Pifithrin-α group ($n = 10$). (B) The epididymis coefficients were significantly decreased in the Pifithrin-α group compared with the control group ($p < .05$), whereas no statistically significant differences were observed in other organ coefficients ($n = 10$)

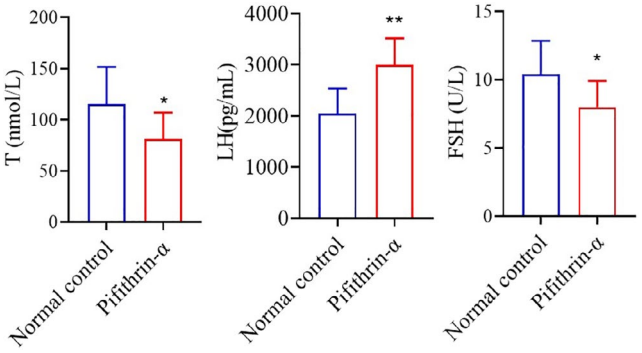

FIGURE 2 Changes in the levels of T, LH, and FSH in mouse serum. Compared with the control group, levels of T and FSH were significantly decreased ($p < .05$), while the LH level of was significantly increased in the Pifithrin-α group ($n = 10$; $p < .01$). FSH, follicle-stimulating hormone; LH, luteinizing hormone; T, testosterone [Colour figure can be viewed at wileyonlinelibrary.com]

3.3 | Sperm quality

As shown in Figure 3C, significant decreases in sperm density and motility were found in the Pifithrin-α group compared with the control group ($p < .05$). Compared with the control group, the percentage of class A and class B sperm were significantly decreased in the Pifithrin-α group ($p < .05$). Sperm collected from the control mice demonstrated normal morphology, counts, and motility (Figure 3B). In addition, a significant increase in the sperm malformation rate occurred in the Pifithrin-α group compared with that in the control group ($p < .01$) (Figure 3C). Furthermore, Figure 3A shows the morphologies of normal and abnormal sperm (abnormal sperm exhibited head or tail defects, such as non-hooked heads, double heads, tail rotation, double tail deformity, etc.).

3.4 | Apoptosis rates

Sperm apoptosis rates were evaluated by flow cytometry. The apoptotic rates of sperm were significantly higher in the Pifithrin-α group compared with the control group ($p < .05$) (Figure 4A).

A TUNEL assay was performed on testis sections to study apoptosis. Spermatogenic cells apoptotic rates were significantly higher in the Pifithrin-α group compared with the control group ($p < .01$) (Figure 4B).

3.5 | Pathological conditions of testicle and epididymal tissue

The morphology of testicular tissue was analyzed by optical microscope and is shown in Figure 5A; black arrows point to the seminiferous tubule lumen, and yellow arrows point to Sertoli cells. In the control group, the seminiferous tubules were arranged compactly and the Sertoli cells were arranged tightly. The spermatogenic cells of different phases could easily be found. However, in the Pifithrin-α group, the spermatogenic cells were disordered, the intercellular space was widened, and vacuoles appear in the cytoplasm of spermatogenic cells. Moreover, mature spermatozoa were reduced (×200). In Figure 5B, red arrows point to the lumen, and green arrows point to epididymal epithelial cells. In the control group, the epididymal structure was clear and intact and lumens were filled with sperm cells. In the Pifithrin-α group, epididymal epithelial cells were severely degenerated and there was a decrease in the number of sperm in the lumen.

3.6 | Testicular ultrastructure

In the control group, the tight junctions (TJs) and apical (ectoplasmic specialization, ES) were intact and neatly arranged. In the Pifithrin-α group, the TJs and apical ES were disordered and partial fragmentation was found. Moreover, the endoplasmic reticulum was dilated (Figure 6B). The basal ES of the Pifithrin-α group were without pathological changes (Figure 6A).

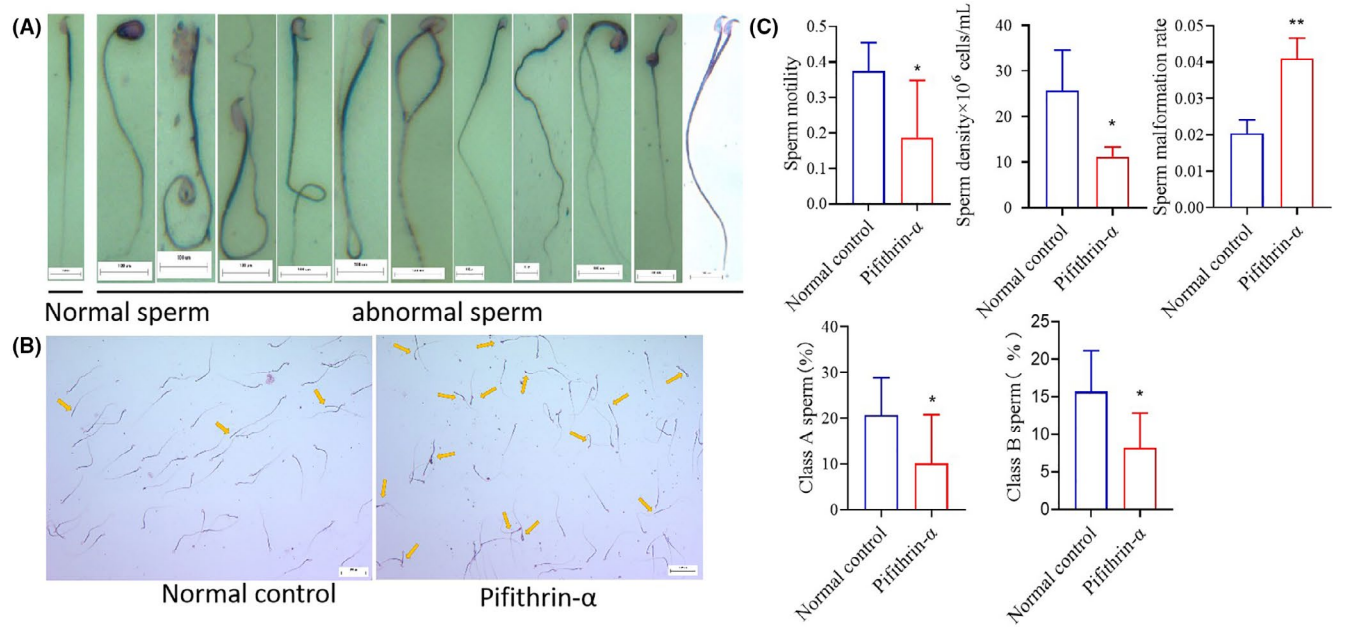

FIGURE 3 Effects of Pifithrin-α on mouse sperm quality parameters and sperm morphology. (A) The morphologies of normal and abnormal sperm (non-hooked heads, double heads, tail rotation, double tail deformity, etc.). (B) Yellow arrows point to malformed sperm. Sperm collected from the control group demonstrated normal morphology, motility, and sperm counts. (C) Compared with the control group, both sperm quantity and motility in the Pifithrin-α group was decreased significantly ($n = 10$; $p < .05$). Compared with the normal control group, the percentage of class A and class B sperm were significantly decreased in the Pifithrin-α group ($p < .05$). The sperm malformation rate of the Pifithrin-α group was significantly higher than that of the control group ($n = 10$; $p < .01$) [Colour figure can be viewed at wileyonlinelibrary.com]

FIGURE 4 Analysis of apoptosis rate of sperm and spermatogenic cells. (A) The spermatozoas in Q1, Q2, Q3, and Q4 represent dead spermatozoas, late apoptotic spermatozoas, early apoptotic spermatozoas, and living spermatozoas, respectively. The sperm apoptosis rate of the Pifithrin-α group was significantly elevated compared with the control group ($n = 3$; $p < .05$). (B) The apoptosis rate of spermatogenic cells in the Pifithrin-α group was significantly elevated compared with the control group ($n = 3$; $p < .01$) [Colour figure can be viewed at wileyonlinelibrary.com]

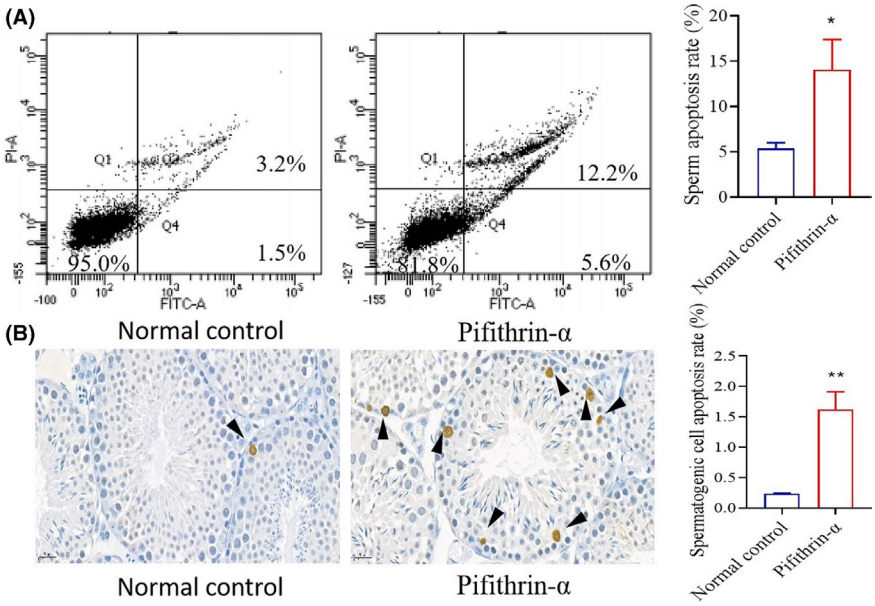

3.7 | Relative mRNA expression levels of *TAp73* and adherence factors

Compared with the control group, the relative mRNA expression of *TAp73* and *Nectin 2* were significantly decreased in the Pifithrin-α group ($p < .01$). Therefore, there was no significant difference in the relative mRNA expression of *ZO-1* between the 2 groups (Figure 7A).

3.8 | The relative protein expression levels of TAp73 and adherence factors

Compared with the control group, the relative protein expression of TAp73 and Nectin 2 was significantly decreased in the Pifithrin-α group ($p < .01$). The relative protein expression of ZO-1 between the 2 groups showed no significant differences (Figure 7B).

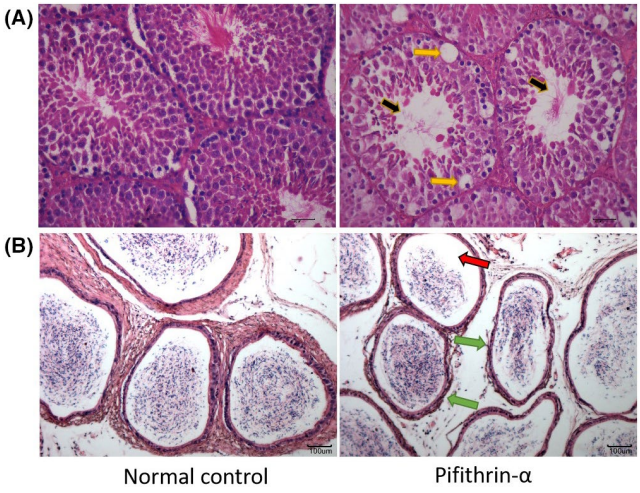

FIGURE 5 Pathological changes in morphology of testicular and epididymal tissue of the mouse. (A) Black arrows point to the seminiferous tubule lumen. Yellow arrows point to Sertoli cells. In the control group, the seminiferous tubules were arranged compactly, and the Sertoli cells were arranged tightly. The spermatogenic cells of different phases could easily be found. However, in the Pifithrin-α group, the spermatogenic cells were disordered, the intercellular space was widened, and vacuoles appear in the cytoplasm of spermatogenic cells. Moreover, mature spermatozoa were reduced (×200). (B) Red arrows point to the lumen. Green arrows point to the epididymal interstitium. In the control group, the structure of epididymal was clear and intact. The lumens were filled with sperm cells. In the Pifithrin-α group, epididymal epithelial cells were severely degenerated and there was a decrease in the number of sperm in the lumen [Colour figure can be viewed at wileyonlinelibrary.com]

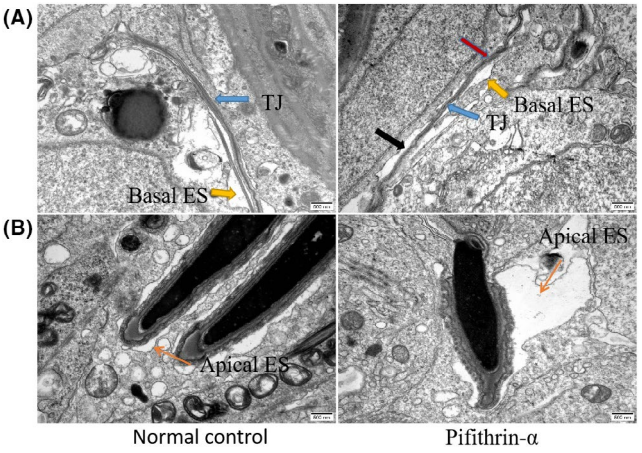

FIGURE 6 Pathological changes in the ultrastructure of mouse testicular tissue. (A) Blue arrows, TJ; yellow arrows, basal ES; black arrows, cleavage of TJ; red arrows, the arrangement of TJ was disordered. In the control group, the TJs were intact and clear, and arranged neatly and tightly. In the Pifithrin-α group, the TJs were disorderly arranged and partial fragmentation was found. There were no pathological changes in basal ES of the Pifithrin-α group (×25 000). (B) Yellow-orange thin arrows, apical ES. In the control group, the apical ES were arranged in order. In the Pifithrin-α group, apical ES were dilated, with disordered arrangement and a loose structure. Moreover, the endoplasmic reticulum was dilated (×25 000). TJ, tight junction; ES, ectoplasmic specialization [Colour figure can be viewed at wileyonlinelibrary.com]

4 | DISCUSSION

Spermatids are closely association with the Sertoli cells until spermatozoa are fully differentiated.[17] Sertoli cells are the only somatic cell type in the spermatogenic tubule and provide germ cells with physical, metabolic, and regulatory support. During all stages of spermatogenesis, germ cells depend on this support by Sertoli cells.[18] The morphological and molecular maturational processes of spermatozoa happen along the Sertoli cell soma.[19] Because of the dynamic reconstruction of the cell-cell connections, germ cells migrate to the lumen through successive detachment and reattachment from Sertoli cells during sperm differentiation.

TJs are essential component of the blood-testis barrier (BTB), which can confine the transmembrane transfer of proteins and lipids in the BTB.[20,21] Through the continuous dissolving and reforming of TJs in BTB, haploid sperm cells differentiate into mature sperm.[22] The tight connection has 2 main functions: forming a barrier and forming a relatively closed space. The Sertoli-germ cell junctions include the ES and the desmosome-like junction, which assist in the translocation of early meiosis spermatocytes from the basement membrane to lumina of the tubules.[23] Therefore, any errors in the adhesion and migration step that occur during spermatogenesis can lead to male infertility.

P73 is a member of the p53 family. *P73* shares structural and functional similarities with *p53*. *TAp73* is an isoform of *p73*. As the key tumor suppressor, the *TAp73* gene has received a lot of attention in suppressing the initiation and progression of tumors.[24] Several studies have demonstrated that *TAp73* participates in the regulation of germ cell differentiation and is a key factor in maintaining male fertility. *TAp73* is the only p53 family member linked to male fertility. *TAp73* plays crucial roles in the regulation of adhesion and maturation of germ cells.[25] *TAp73*-knockout mice showed reduced sperm density, motility, and testicular weight, and increased apoptosis of germ cells. In addition, the expression of *tissue inhibitor of metalloproteinases 1* (*Timp 1*) and *serine protease inhibitor 3n* (*Serpin 3n*) were significantly increased. Meanwhile, the spermatogenic cells were disorderly arranged, the spermatogenic epithelium became thinner, and the seminiferous tubules were devoid of mature spermatozoa. The arrangement of the apical ES was disordered, and the cytoplasmic arm of Sertoli was relatively short and thin; the degenerative vacuoles could be obviously seen after *TAp73* knockdown.[9] Due to the abnormal shape of Sertoli cells, they could not envelop germ cells. Germ cell adhesion and BTB integrity had been disrupted, and only a small number of separated, loosely attached germ cells could be seen in the seminiferous tubules. This appeared to result in germ cells being prematurely sloughed off the seminiferous epithelium and dying by apoptosis, ultimately leading to a severe depletion of germ cells and mature spermatozoa.[26] Our results showed that sperm quality parameters significantly decreased and spermatogenic

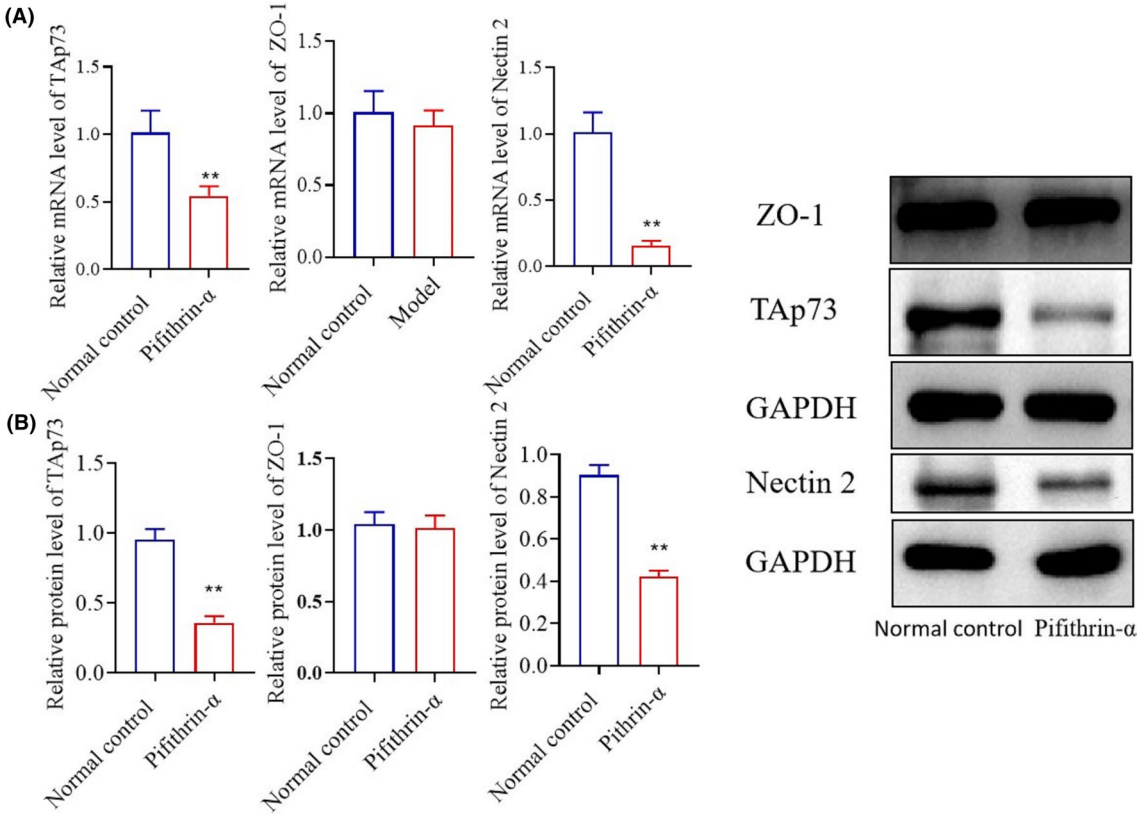

FIGURE 7 Effects of Pifithrin-α on relative mRNA and protein expression levels of *TAp73* and adherence factors in the mouse. (A) Compared with the control group, the relative mRNA expression of *TAp73* and *Nectin 2* were significantly decreased in the Pifithrin-α group ($n = 3$; $p < .01$). The relative mRNA expression of *ZO-1* was not significantly different between the 2 groups. (B) Compared with the control group, the relative protein expression of TAp73 and Nectin 2 was significantly decreased in the Pifithrin-α group ($n = 3$; $p < .01$). The relative expression of ZO-1 was not significantly different between the 2 groups [Colour figure can be viewed at wileyonlinelibrary.com]

cell arrangement was disordered. There was also disruption of TJs seen in some areas after 30 days of intraperitoneal application in mice. Moreover, the arrangement of apical ES was disordered and the endoplasmic reticulum was dilated, while germ cells appeared to prematurely slough off the seminiferous epithelium or develop into malformed spermatozoa. This indicates that adhesion and migration between spermatogenic and Sertoli cells could be impeded by inhibiting the gene expression of *TAp73* during spermatogenesis. Our results were consistent with earlier reports.[27] The model performance was consistent with the clinicopathological features of this disease, indicating that the model is successful. Studies on relevant connexins and regulators have demonstrated that the relative protein and mRNA expression of *TAp73* and *Nectin 2* were significantly decreased in the Pifithrin-α group. However, no significant difference was observed in the relative protein and mRNA expression of *Zonula occludens-1* (*ZO-1*).

Occludins, claudins, and ZO-1 are the main proteins in the TJs of Sertoli cells.[28] ZO-1 is a membrane protein, which usually interacts with occludin to form complexes and exert barrier functions.[29] Nectin-2 is an adhesion molecule localized exclusively at ES. Studies have revealed that abnormal expression of Nectin-2 protein in testis tissue leads to male infertility.[30] ES consists of Nectin-2, N-cadherin, and E-cadherin.[31,32] We therefore speculated that the inhibition of *TAp73* expression resulted in the loss of apical ES integrity and defects in the adhesion and migration between spermatogenic and Sertoli cells during spermatogenesis.

Taken together, these results suggest that we successfully established an oligoasthenospermia model by intraperitoneal injection of Pifithrin-α. The model could inhibit *TAp73* gene expression and concomitantly affect spermatogenic and Sertoli cells. Subsequently, *TAp73* inhibition resulted in the disruption of apical ES and TJ integrity that caused the defects in the adhesion and migration between spermatogenic and Sertoli cells and ultimately lead to oligoasthenospermia. These results provide a new idea for further investigating the pathogenesis of oligoasthenospermia. The successful establishment of this model provides a new research object for the development of novel and effective agents for the treatment of oligoasthenospermia.

ACKNOWLEDGEMENTS

This work was supported by the National Natural Science Foundation of China (NSFC, No 82174162); Natural Science Foundation of Anhui Provincial Department of Eduction (No KJ2020A0386.

CONFLICT OF INTEREST

The authors declare that they have no conflict of interests.

AUTHOR CONTRIBUTIONS

All listed authors have participated in the study and meet the requirements for publication.

ORCID

Hong-Juan Liu https://orcid.org/0000-0002-5557-6467

REFERENCES

1. Zhang T, Wang X, Wang Z, et al. A diagnostic model to improve the predictability of natural pregnancy potential in patients with oligoasthenospermia. *Med Sci Monit*. 2020;26:e922316.
2. Jungwirth A, Giwercman A, Tournaye H, et al; European Association of Urology Working Group on Male Infertility. European Association of Urology guidelines on Male Infertility: the 2012 update. *Eur Urol*. 2012;62(2):324-332.
3. Zou D, Meng X, Wang B, et al. Analysis of pharmacological mechanisms and targets mining of Wuzi-Yanzong-Wan for treating non-obstructive oligoasthenospermia. *Biomed Pharmacother*. 2019;115:108898.
4. Fainberg J, Kashanian JA. Recent advances in understanding and managing male infertility. *F1000Res*. 2019;8:F1000 Faculty Rev-670.
5. Wang C, Sang M, Gong S, Yang J, Cheng C, Sun F. Two resveratrol analogs, pinosylvin and 4,4′-dihydroxystilbene, improve oligoasthenospermia in a mouse model by attenuating oxidative stress via the Nrf2-ARE pathway. *Bioorg Chem*. 2020;104:104295. http://dx.doi.org/10.1016/j.bioorg.2020.104295
6. An Q, Zhang K, Fu L, et al. The impact of exogenous testosterone supplementation on spermatogenesis in a rat model of oligoasthenospermia. *Int J Clin Exp Pathol*. 2020;13(6):1287-1299.
7. Wang CN, Sang MM, Gong SN, Yang JF, Cheng CY, Sun F. Two resveratrol analogs, pinosylvin and 4,4'-dihydroxystilbene, improve oligoasthenospermia in a mouse model by attenuating oxidative stress via the Nrf2-ARE pathway. *Bioorg Chem*. 2020;104:104295.
8. Zhang P, Liu F, Adi L, Yi M. Research progress on the establishment of oligoasthenospermia animal model. *J Xinjiang Med Univ*. 2014;37(08):974-976+980.
9. Inoue S, Tomasini R, Rufini A, et al. TAp73 is required for spermatogenesis and the maintenance of male fertility. *Proc Natl Acad Sci U S A*. 2014;111(5):1843-1848.
10. Xu Z, Zhang F, Zhu Y, et al. Traditional Chinese Medicine Ze-Qi-Tang formula inhibit growth of non-small-cell lung cancer cells through the p53 pathway. *J Ethnopharmacol*. 2019;234:180-188.
11. Chen J. Effect of okra polysaccharide on the spermatogenesis of KKAy mice. *Int J Biol Macromol*. 2019;140:98-101.
12. Ren Y, Shao W, Zuo L, et al. Mechanism of cadmium poisoning on testicular injury in mice. *Oncol Lett*. 2019;18(2):1035-1042.
13. Mahmoud YI. Effect of extract of Hibiscus on the ultrastructure of the testis in adult mice. *Acta Histochem*. 2012;114(4):342-348.
14. Li L, Wu DL, Dai N, et al. The effect of Atractylodes on rat sperm mitochondrial membrane potential and apoptosis in vitro. *Pharmacol Clinic Chinese Materia Medica*. 2019;35(05):25-30.
15. Azad F, Nejati V, Shalizar-Jalali A, Najafi G, Rahmani F. Antioxidant and anti-apoptotic effects of royal jelly against nicotine-induced testicular injury in mice. *Environ Toxicol*. 2019;34(6):708-718.
16. Qian C, Meng Q, Lu J, Zhang L, Li H, Huang B. Human amnion mesenchymal stem cells restore spermatogenesis in mice with busulfan-induced testis toxicity by inhibiting apoptosis and oxidative stress. *Stem Cell Res Ther*. 2020;11(1):290.
17. Cannarella R, Condorelli RA, Mongioì LM, La Vignera S, Calogero AE. Molecular biology of spermatogenesis: novel targets of apparently idiopathic male infertility. *Int J Mol Sci*. 2020;21(5):1728.
18. Kjærner-Semb E, Ayllon F, Kleppe L, et al. Vgll3 and the Hippo pathway are regulated in Sertoli cells upon entry and during puberty in Atlantic salmon testis. *Sci Rep*. 2018;8(1):1912.
19. Griswold MD. 50 years of spermatogenesis: Sertoli cells and their interactions with germ cells. *Biol Reprod*. 2018;99(1):87-100.
20. Li XY, Zhang Y, Wang XX, et al. Regulation of blood-testis barrier assembly in vivo by germ cells. *FASEB J*. 2018;32(3):1653-1664.
21. Zhao L, Yao C, Xing X, et al. Single-cell analysis of developing and azoospermia human testicles reveals central role of Sertoli cells. *Nat Commun*. 2020;11(1):5683.
22. Wen Q, Tang EI, Li N, et al. Regulation of blood-testis barrier (BTB) dynamics, role of actin-, and microtubule-based cytoskeletons. *Methods Mol Biol*. 2018;1748:229-243.
23. Mruk DD, Cheng CY. The mammalian blood-testis barrier: its biology and regulation. *Endocr Rev*. 2015;36(5):564-591.
24. Gomes S, Raimundo L, Soares J, et al. New inhibitor of the TAp73 interaction with MDM2 and mutant p53 with promising antitumor activity against neuroblastoma. *Cancer Lett*. 2019;446:90-102.
25. Nemajerova A, Moll UM. Tissue-specific roles of p73 in development and homeostasis. *J Cell Sci*. 2019;132(19):jcs233338.
26. Abud HE, Hime GR. Regulation of cell adhesion in the testis: a new role for p73. *Asian J Androl*. 2014;16(6):799-800.
27. Lu Y, Liu M, Tursi NJ, et al. Uropathogenic *Escherichia coli* infection compromises the blood-testis barrier by disturbing mTORC1-mTORC2 balance. *Front Immunol*. 2021;12:582858.
28. Li L, Gao Y, Chen H, et al. Cell polarity, cell adhesion, and spermatogenesis: role of cytoskeletons. *F1000Res*. 2017;6:1565.
29. Su L, Wang Z, Xie S, et al. Testin regulates the blood-testis barrier via disturbing occludin/ZO-1 association and actin organization. *J Cell Physiol*. 2020;235(9):6127-6138.
30. Liu B, Shen LJ, Zhao TX, et al. Automobile exhaust-derived $PM_{2.5}$ induces blood-testis barrier damage through ROS-MAPK-Nrf2 pathway in Sertoli cells of rats. *Ecotox Environ Safe*. 2020;189:110053.
31. Wu D, Huang CJ, Jiao XF, et al. Olaquindox disrupts tight junction integrity and cytoskeleton architecture in mouse Sertoli cells. *Oncotarget*. 2017;8(51):88630-88644.
32. Zhang X, Lui WY. Dysregulation of nectin-2 in the testicular cells: an explanation of cadmium-induced male infertility. *Biochim Biophys Acta*. 2014;1839(9):873-884.

How to cite this article: Liu H-J, Deng M-Y, Zhu Y-Y, et al. Establishment of an oligoasthenospermia mouse model based on *TAp73* gene suppression. *Anim Models Exp Med*. 2021;4:351–358. doi:10.1002/ame2.12186